

Electronic Supplementary Information

Functional silsesquioxane-based hierarchical assemblies for antibacterial/antifungal coatings

Irina-Elena Bordianu,^a Geta David,^b Bogdana Simionescu,^c Magda Aflori,^a Cristian Ursu,^a
Adina Coroaba,^a Gabriela Hitruc,^a Corneliu Cotofana^a and Mihaela Olaru*^a

^a "Petru Poni" Institute of Macromolecular Chemistry, 41A Gr. Ghica Voda Alley, 700487 Iasi, Romania. Fax: 0040211299; Tel:0040232217454; Email: olaruma@icmpp.ro

^b "Gh. Asachi" Technical University of Iasi, Department of Natural and Synthetic Polymers, 700050 Iasi, Romania

^c "Costin D. Nenitescu" Centre of Organic Chemistry, 202B Splaiul Independentei, 71141 Bucharest, Romania

Materials and methods: All reagents (trimethoxysilyl)propylmethacrylate (TMSPMA), dodecylamine (DDA), silver nitrate (AgNO₃), titanium isopropoxide (TIP)) were purchased from Sigma Aldrich and used without purification. Three standard strains (one Gram-positive bacterium, one Gram-negative bacterium and one fungus) were taken into account for the antibacterial/antifungal tests using the agar diffusion method: *Staphylococcus aureus* ATCC 25923, *Escherichia coli* ATCC 25922 and *Candida albicans* ATCC 10231. All microorganisms were stored at -80 °C in 10 % glycerol. The bacteria were refreshed in Mueller-Hinton broth (Merck, Germany) at 36 °C and afterward inoculated on Plate Count plates (Biokar, France) for checking purity. Fungi were refreshed on Sabouraud dextrose agar (SDA) (Biokar, France) and were grown at 36 °C. The microbial suspensions were prepared with these cultures in sterile saline solution and compared to the 0.5 McFarland standard, yielding for all microorganisms a suspension containing approx. 1×10^8 CFU/mL. Volumes of 0.2 mL from each inoculum were spread onto a Mueller-Hinton Agar pre-poured in Petri plates. After drying, the cover slips coated with the polymer films were added. To evaluate the antibacterial/antifungal properties, the inhibition of growth was measured under standard conditions after 24 hours of incubation at 36 °C. The measurements of the antibacterial/antifungal properties were realized three months after

the synthesis, to evidence the stability of the polymers from this perspective.

The surface composition analysis was studied by XPS (ESCALAB 220i-XL, VG, UK) using a monochromated Al K α source (1486.6 eV) and a pass energy of 180 eV at a base pressure of 2×10^{-9} mbar. The crystallographic structure of the samples was studied with a D8 Advance Bruker AXS Diffractometer (XRD). The X rays were generated using a CuK α source with an emission current of 36 mA and a voltage of 30 kV. Scans were collected over the $2\theta = 2 - 40^\circ$ range using a step size of 0.02° and a count time of 0.2 s/step. The semi-quantitative analysis was performed with an EVA soft from DiffracPlus package and an ICDD-PDF2 database based on patterns relative heights. SEM micrographs were obtained with a Quanta 200 scanning probe microscope, the specimens being fixed using adhesive paste on Al conducting supports of cylindrical shapes and then sputter-coated with gold. AFM height measurements and phase imaging were performed in air, at room temperature, in phase contrast tapping mode, using a scanning probe microscope Solver PRO-M with commercially available NSG10 cantilever (NT-MDT, Zelenograd, Moscow, Russia). The manufacturer value for the probe tip radius was 10 nm and the typical force constant was 11.8 N/m. The resonance frequency of the cantilever was 180 KHz. For image acquisition and analysis Nova v.1.26.0.1443 for Solver software, NT-MDT Russia, was used. Small amounts of diluted samples dropped on carbon coated grids were analyzed with a HT7700 Transmission Electron Microscope in a 100 KV High Resolution Mode. Water vapours sorption capacity of the gel samples was measured by using the fully automated gravimetric analyzer IGA-sorp supplied by Hiden Analytical, Warrington (UK). Water vapours sorption capacity of the samples at 25 °C in the 0-90 % relative humidity range (RH) was investigated on an IGA-sorp equipment. The drying of the samples before sorption measurements was carried out at 25 °C in flowing nitrogen (250 mL min^{-1}) until the weight of the sample was in equilibrium at $\text{RH} < 1 \%$.

WAXD spectroscopy: the WAXD diagrams (Fig. S1) reveal the presence of several peaks for both hybrid nanocomposites, indicating the coexistence of crystalline and amorphous units, although crystallinity is not high for POSS-Ag and excludes the formation of solely cage structures (caged silsesquioxanes are normally crystallizable). The qualitative XRD analysis of POSS-AgTi indicate that titania nanoparticles are present only in the anatase form. Moreover, the silver contained in both silsesquioxane-based hybrid nanocomposites presents a high percentage of {111} facets. As follows, the presence of two peaks at $2\theta = 38.2^\circ$ and 44.1°

corresponding to {111} and {200} crystalline planes of face-centered cubic (fcc) silver can be evidenced.

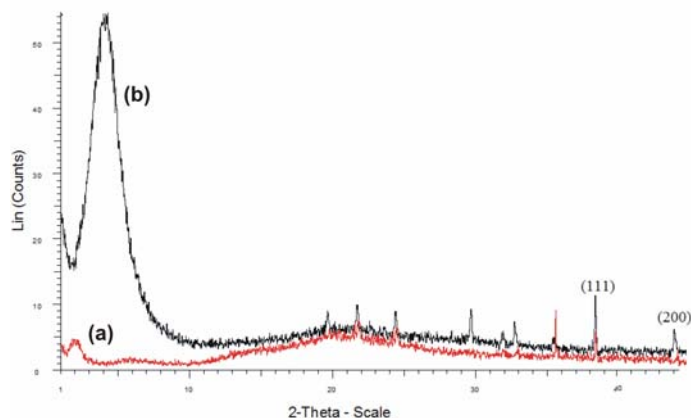


Fig. S1 XRD patterns. (a) POSS-Ag. (b) POSS-AgTi.

XPS measurements: XPS data of POSS-Ag and POSS-AgTi are shown in Fig. S2 and Tab. S1, respectively. The studied compounds are mainly composed of C, O, Ag and N, with surprisingly less Ti and Si content. The C 1s spectra of POSS-Ag and POSS-AgTi took into consideration the presence of the peaks attributed to C-C/C-Si, C-O/C-N, C=O and O-C=O species. The higher content of oxygen as concerning the silica (the molar ratio of Si to O in silsesquioxane units is 1:1.5) may be attributed to the existence of higher amounts of hydroxyl units and water adsorbed on silica surface, while the small content of titanium in POSS-AgTi can be explained assuming that silver is basically covering the film substrate. A small amount of sulphur (between 0.64 and 1.77 % for POSS-Ag and POSS-AgTi, respectively), mainly due to the presence of trace amounts of peroxides in isopropyl alcohol which influence the conversion of absorbed sulfur dioxide to sulfate was also evidenced. The binding energy of S2p signal (168.3 eV) is assigned to the SO_4^{2-} ions. Moreover, the presence of the binding energy of S2p signal at the same value for both compounds rules out the sulfur doping of TiO_2 , i.e., the formation of Ti-S bonds (which usually appear at 164.8 eV), being known that sulfur is one of the compounds that may influence TiO_2 photocatalytic activity. As for nitrogen, XPS spectra evidence the presence of three peaks, two of them related to the nitrogen TiO_2 -doped compounds, i.e., the nitrogen doped into TiO_2 lattice (N-Ti-O bond, 398.9 eV) and the nitrogen chemically adsorbed on TiO_2 surface (Ti-O-N, 400.1 eV), and one to the nitrogen belonging to C-N bond (399.2 eV). Although the presence of both states of nitrogen TiO_2 -doped compounds plays an important role in the improvement of

TiO₂ photocatalytic properties, a higher amount of N-Ti-O bonds is required to increase the photocatalytic activity under visible light. In the present study, the higher amount of the nitrogen chemically adsorbed on TiO₂ surface (peak area: 77.92 %) as compared to the nitrogen doped into the TiO₂ lattice (peak area: 13.05 %) is restraining the photocatalytic performances since the chemically adsorbed nitrogen is practically covering the TiO₂ surface, therefore decreasing the number of active sites. O1s spectra of POSS-Ag show the contributions of four components. The main component is the peak from 532.5 eV ascribed to the oxygens from Si-O-Si bonds, followed by the presence of hydroxyl units from Si-OH at 531.5 eV, O=C-O and C-O units from methyl methacrylate at 533.8 and 534.4 eV, respectively. The Si2p peak observed at around 101.8 eV may be related to the presence of O-Si-C bonds, while the one from 102.6 eV can be assigned to Si-O of the siloxane network. For POSS-AgTi, two types of Si2p peaks were detected at 101.2 and 102.2 eV, assigned to the presence of both Si from Si-O-Si network and Si of the Ti-O-Si bond, respectively. The O1s spectra show the contributions of four components: the main component is the peak from 532.6 eV, assigned to a combination of the oxygens belonging to Ti-O-Si and Si-O-Si bonds, respectively, followed by the presence of hydroxyl units from Si-OH and Ti-OH, respectively, at 531.5 eV, O-Ti units at 530.9 eV and C=O from methyl methacrylate at 533.8 eV. The shift of the binding energy of C=O groups from both silsesquioxane-based polymers as compared to the standard O1s binding energy of C=O units, i.e., 532.1 eV, can be attributed to the electrostatic interaction between carbonyl oxygen and the surface of silver nanoparticles.¹ Two chemically distinct Ag3d components are observed for both silsesquioxane-based hybrid nanocomposites with titanium and/or silver content. The low binding energy component (between 368.6 - 368.7 eV) is attributed to electron emission from metallic silver (Ag⁰ – peak area: 96.82 % and 85.70 % for POSS-Ag and POSS-AgTi, respectively), while the high binding energy component (374.7 and 374.6 eV for POSS-Ag and POSS-AgTi, respectively) arises from silver ions indicating that a small fraction of unreduced Ag⁺ remains on samples surface (Ag⁺ – peak area: 3.18 % and 14.30 % for POSS-Ag and POSS-AgTi, respectively). Furthermore, these binding energies are smaller than the ones corresponding to metal silver (368.2 eV and 374.2 eV for Ag 3d_{5/2} and for Ag 3d_{3/2}, respectively) but higher than the binding energy of Ag₂O (367.5 eV and 373.5 eV for Ag 3d_{5/2} and for Ag 3d_{3/2}, respectively),² this indicating the interaction between oxygen atoms from carbonyl groups and surface of silver nanoparticles, as well. The shift of Ag3d_{5/2} peak from POSS-AgTi to lower

binding energy values cannot be related to an increase in size of silver nanoclusters, therefore one may attribute this process to both electron transfer from TiO₂ to metallic silver and from silver particles to silica. POSS-AgTi surface shows two peaks of Ti2p_{1/2} (458.2 eV) and Ti2p_{3/2} (459.1 eV), which are assigned to Ti⁴⁺ oxidation state of pure TiO₂ as well as to Ti⁴⁺ involved in Si-O-Ti bond. The decrease of electron density around Ti atom due to the presence of more electronegative Si atoms induces an increase of Ti binding energies as compared to pure TiO₂. On the other hand, one cannot exclude the possibility of electrons transfer from TiO₂ to silver nanoclusters, being known that the presence of Ag⁰ on titania nanotubes gradually shifts the binding energy of Ti⁴⁺ atoms to higher energy values due to the influence of accumulated electrons on the generation of holes (h⁺) on TiO₂ surface. Moreover, TiO₂ may provide electrons which can reduce Ag⁺ to Ag⁰ or can be accumulated on Ag⁰ nanoparticles. Usually, the presence of small amounts of silver atoms in TiO₂-based compounds enhances the photocatalytic efficiency of TiO₂, these atoms acting as electron traps and increasing the separation between the holes and the photoelectrons. Although a small amount of silver (6 TIP: 0.1 AgNO₃ molar ratio) was used in the preparation of POSS-AgTi, the molar ratio of Ag/Ti at the surface is much higher (15.7), meaning that silver species are highly concentrated on the surface. Therefore, a lower efficiency of TiO₂ photocatalytic activity in the visible domain is to be expected, since a high surface area is covered by silver which acts as a barrier that prevents, on one hand, TiO₂ light absorption and organic substrates to contact the TiO₂ surface and, on the other hand, the silver in excess to form recombination centers for electron-hole pairs.

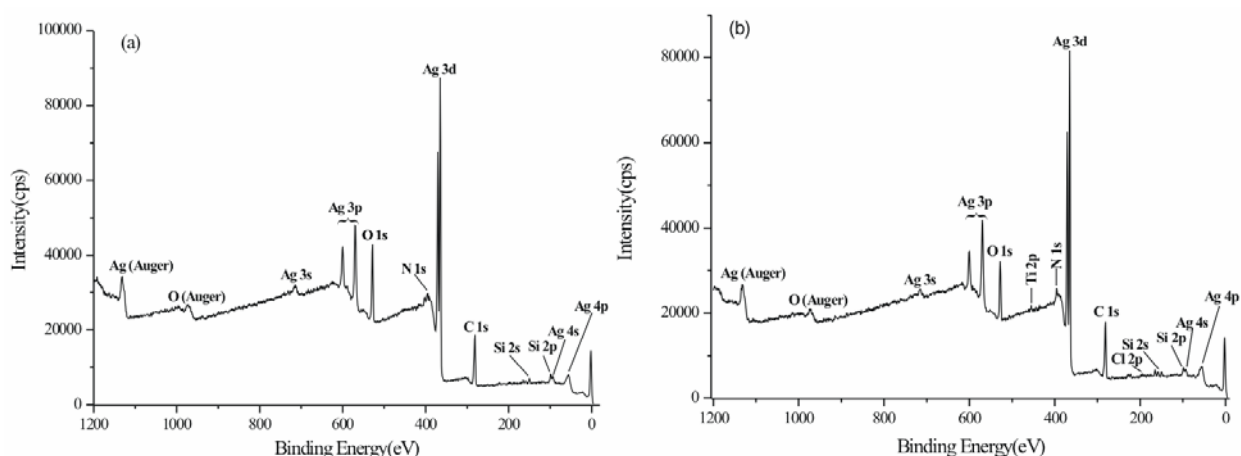


Fig. S2 High-resolution XPS spectra. (a) POSS-Ag. (b) POSS-AgTi.

Table S1 Contents of functional groups of POSS-Ag and POSS-AgTi (BE – binding energy (eV), PC - percentage (%))

Functional group			Samples	
			POSS-Ag	POSS-AgTi
C 1s	C-C/C-Si	BE	285	285
		PC	70.69	71.45
	C-N/C-O	BE	286.5	286.4
		PC	16.21	14.66
	C=O	BE	287.8	287.4
		PC	6.62	6.09
	O-C=O	BE	289	288.9
		PC	6.48	7.8
O 1s	O-Ti	BE	-	530.9
		PC	-	13.42
	OH-Si	BE	531.5	531.5
		PC	16.53	27.27
	Si-O-Si	BE	532.5	-
		PC	56.61	-
	Si-O-Si/ Ti-O-Si	BE	-	532.6
		PC	-	46.18
	O-C	BE	533.7	533.8
		PC	18.09	13.13
	O-C=O	BE	534.9	-
		PC	8.77	-
Ag 3d	Ag ⁰	BE	368.7	368.6
		PC	96.82	85.70
	Ag ⁺	BE	374.7	374.6
		PC	3.18	14.30
Si 2p	O-Si-C/ Si-O-Si	BE	101.8	101.2
		PC	9.97	18.33
	Si-O-Si	BE	102.6	-
		PC	90.03	-
	Si-O-Si/ Ti-O-Si	BE	-	102.2
		PC	-	81.67
S 2p	SO ₄ ²⁻	BE	168.3	168.3
		PC	0.64	1.77
N 1s	N-Ti-O	BE	-	398.9
		PC	-	13.05
	Ti-O-N	BE	-	400.1
		PC	-	77.92
	N-C	BE	399.4	399.2
		PC	64.4	9.03
	N-O	BE	400.7	-
		PC	35.6	-
Ti 2p _{3/2}	O-Ti from TiO ₂	BE	-	459.1
		PC	-	81.61
	Si-O-Ti	BE	-	458.2
		PC	-	18.39

Determination of antimicrobial/antifungal properties: Similarly to silver ions, the silver nanoparticles penetrate bacteria membrane and interact with sulfur- and phosphorous-containing compounds like proteins and DNA, thus leading to the death of the bacterial cells. However, the detailed mechanism on the antimicrobial activity of silver nanoparticles – different from the one characteristic to bulk metallic or ionic forms of silver – is not yet fully understood. Until now, three main mechanisms were proposed to explain the antibacterial activity: (i) release of silver ions upon dissolution, (ii) generation of reactive oxygen species at the surface of silver nanoparticles in the presence of molecular oxygen, and (iii) surface reactivity due to the presence of several crystal defects. It is still unclear whether the above mentioned mechanisms act independently or simultaneously. Both silsesquioxane-based hybrid nanocomposites were active against a Gram-positive bacterium (*Staphylococcus aureus*), a Gram-negative bacterium (*Escherichia coli*) and one fungus (*Candida albicans*). The results, evaluated after three months (Fig. S3, Tab. S2), indicate that the coatings with POSS-AgTi were more likely to display higher antimicrobial activity than the ones with POSS-Ag. As follows, POSS-AgTi exhibited a larger inhibition zone, i.e., 15 mm and 13 mm in case of *Candida albicans* and *Escherichia coli*, respectively, while for *Staphylococcus aureus* presented a similar inhibition zone with the one exerted by POSS-Ag, i.e., 12 mm. As for POSS-Ag, the corresponding values of the inhibition zone were 12.5 mm in case of *Candida albicans* and 12 mm for both *Escherichia coli* and *Staphylococcus aureus*, respectively.

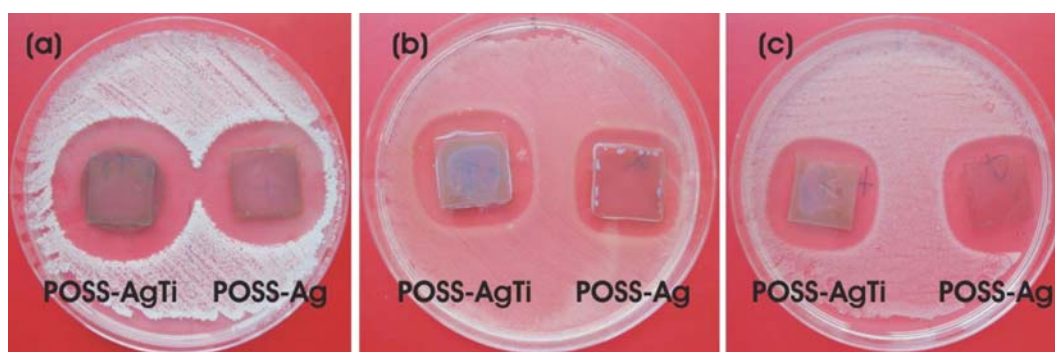


Fig. S3 Antimicrobial response of POSS-Ag and POSS-AgTi. (a) *Candida albicans*. (b) *Escherichia coli*. (c) *Staphylococcus aureus*.

Table S2 Measurements of the inhibition zone illustrating the antibacterial/antifungal responses of POSS-Ag and POSS-AgTi

Microorganism	<i>Staphylococcus aureus</i>		<i>Escherichia coli</i>		<i>Candida albicans</i>	
Sample	POSS-AgTi	POSS-Ag	POSS-AgTi	POSS-Ag	POSS-AgTi	POSS-Ag
Inhibition zone	12 mm	12 mm	13 mm	12 mm	15 mm	12.5 mm

Determination of POSS-AgTi photocatalytic activity under UV irradiation: Upon UV (wavelength less than 400 nm) irradiation of anatase phase from titanium-based compounds the electrons from the valence band get excited to the conduction band and lead to the formation of positive holes (h^+). Both the electrons from the conduction band and the holes from the valence band may interact with water and molecular oxygen, yielding reactive hydroxyl radicals (HO^\cdot) and superoxide anions ($O_2^{\cdot-}$). The generation and the subsequent reactions involving these highly reactive radicals are considered to represent the main degradation pathways of different organic substrates in oxygenated aqueous solutions. Evaluation of the POSS-AgTi film photocatalytic activity (Fig. S4, Scheme S1) was performed through the photocatalytic degradation of coumarin under excimer laser irradiation (248 nm) *via* the generation of HO^\cdot radicals. When reacting with hydroxyl radicals, coumarin (a fluorophore with poor fluorescence) follows the hydroxylation reaction to a strong fluorescent derivative, i.e., 7-hydroxycoumarin. The UV-vis spectrum of an aqueous solution of coumarin ($c = 1.24 \times 10^{-4}$ M) evidences the presence of two strong absorption bands, assigned to $\pi - \pi^*$ and $n - \pi^*$ transitions, at 276 nm and 306 nm. The fluorescence spectrum of the aqueous solution of coumarin ($\lambda_{exc} = 306$ nm) exhibits the presence of only one emission band located at 393 nm, that can be attributed to the presence of neutral coumarin molecules. Upon irradiation of POSS-AgTi film immersed in the aqueous solution of coumarin, the fluorescence spectra of coumarin show two emission bands located at around 402 nm and 445 nm, respectively, which can be assigned to neutral and tautomer anion of 7-hydroxycoumarin species in the excited single state formed following the reaction of coumarin with HO^\cdot (Fig. S4, Scheme S1), the yields of 7-hydroxycoumarin being reported as being around 4.7 % per generated HO^\cdot . The bands position was not affected by the pulse numbers, i.e., 400, 600 and 800 pulses at a laser fluence of 140 mJ/cm^2 , the intensity of these bands increasing with increasing laser pulses. The formation of the tautomer anion was promoted due to 7-

hydroxycoumarin proton dissociation in water, a solvent with excellent hydrogen-bonding solvation ability.

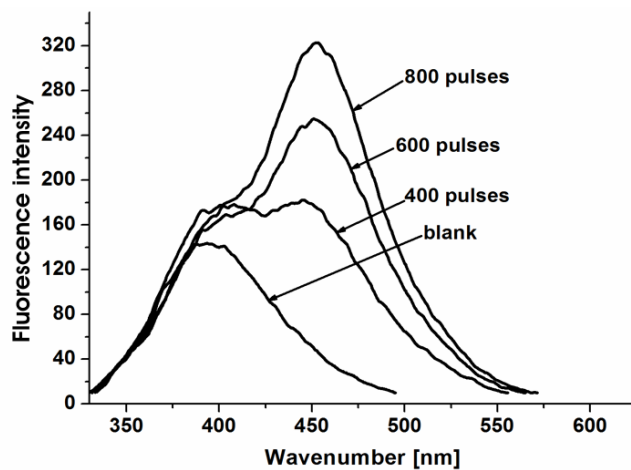
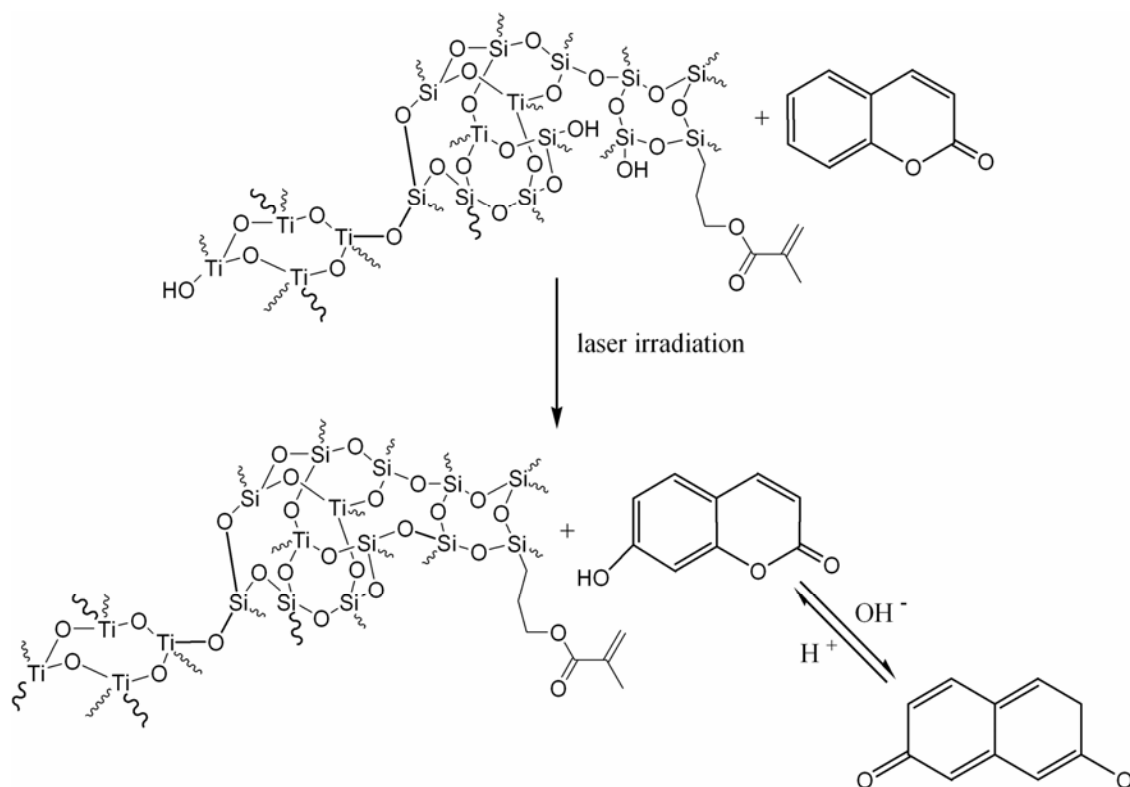


Fig. S4 Determination of POSS-AgTi photocatalytic activity under UV irradiation.



Scheme S1 Formation of 7-hydroxycoumarin upon hydroxylation reaction in the presence of POSS-AgTi.

Permeability measurements: The average pore size and the specific surface area of the synthesized compounds were determined by measuring the water vapors sorption capacity of the gel samples (Fig. S5, Tab. S3). The values of water vapor sorption capacities for both samples are very low, i.e., 4.44 and 2.16 for POSS-Ag and POSS-AgTi, respectively. According to IUPAC classification, the obtained sorption/desorption isotherms can be related to type V curves describing the sorption of hydrophobic/low hydrophilic materials with weak sorbent–water interactions, low sorption at low relative humidity and, sometimes, moderate sorption at the middle relative humidity, followed by a suddenly high water sorption at a relative humidity close to 100. This type of sorption isotherm is characteristic to porous materials. The two isotherms show hysteresis between the sorption and desorption cycles at low and medium humidity levels due to the effect of the crystallinity degree. Moreover, the final mass was not similar to the initial one, this indicating the retention of a specific amount of sorbed water in the silsesquioxanes cages bound through hydrogen bonds. While the sorption or desorption equilibrium is reached almost in every step for POSS-Ag, the pre-established time for POSS-AgTi was too short. Due to silver deposition onto titania nanoparticles, BET surface area of POSS-AgTi (28 m²/g) has been reduced significantly as compared to the POSS-Ag one (62 m²/g).

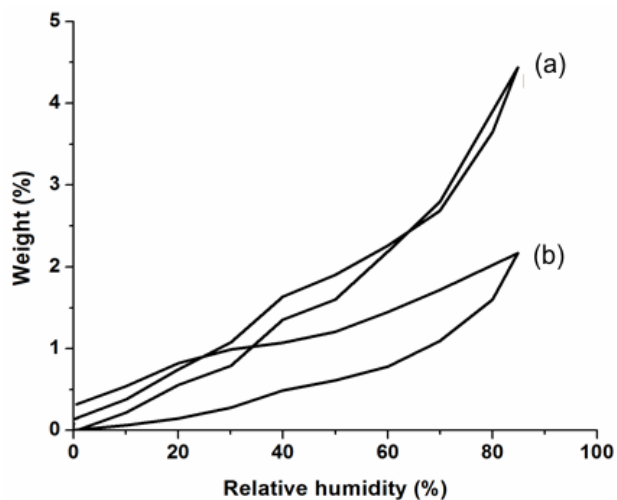


Fig. S5 Measurements of water vapors sorption capacity. (a) POSS-Ag. (b) POSS-AgTi.

Table S3 Estimated values of the GAB and BET models parameters for POSS-Ag and POSS-AgTi.

Sample	Average pore size (nm)	Weight (% d.b.)	BET analysis	
			A _{BET} (m ² /g)	Monolayer (g/g)
POSS-Ag	1.43	4.4386	62.079	0.017681
POSS-AgTi	1.52	2.1665	28.578	0.008140

References

- 1 H. H. Huang, X. P. Ni, G. L. Loy, C. H. Chew, K. L. Tan, F. C. Loh, J. F. Deng and G. Q. Xu, *Langmuir*, 1996, **12**, 909.
- 2 J. F. Moulder, J. Chastain and R. C. King, *Handbook of X-ray Photoelectron Spectroscopy: A Reference Book of Standard Spectra for Identification and Interpretation of XPS Data*; Physical Electronics: Eden Prairie, MN, 1995.